Solar Energy 163 (2018) 62–69

Contents lists available at ScienceDirect

Solar Energy

journal homepage: www.elsevier.com/locate/solener

Differential degradation patterns of photovoltaic backsheets at the array level☆

Andrew Fairbrother[a,*], Matthew Boyd[a], Yadong Lyu[a], Julien Avenet[a], Peter Illich[a], Yu Wang[b], Michael Kempe[c], Brian Dougherty[a], Laura Bruckman[b], Xiaohong Gu[a,*]

[a] Engineering Laboratory, National Institute of Standards and Technology (NIST), Gaithersburg, MD 20899, USA
[b] SDLE Research Center, Materials Science & Engineering, Case Western Reserve University, Cleveland, OH 44106, USA
[c] National Renewable Energy Laboratory (NREL), Golden, CO 80401, USA

ARTICLE INFO

Keywords:
Photovoltaic array
Field survey
Reliability
Backsheet degradation
Exposure conditions
Polyethylene naphthalate

ABSTRACT

There are relatively few field studies on the degradation of non-fluoropolymer-based backsheets, and understanding their in-field behavior is critical for further development of such products. In this study, backsheet degradation of modules with one of these new types of backsheets (polyethylene naphthalate (PEN)-based) was documented at a four-year old utility-scale array located in Maryland (USA). Visual inspection, colorimetry, glossimetry, and Fourier-transform infrared spectroscopy (FTIR) revealed highly varied properties depending on module position within the array. Specifically, modules near the edge of the array and with higher mounting elevations underwent greater amounts of backsheet degradation, as indicated by yellowing and gloss-loss. The reason for these unique degradation patterns were differential backside exposure conditions, especially of ultraviolet light. This was strongly influenced by the array design, including array structural and environmental factors, such as module spacing and ground cover, respectively. Within the array, no clear link between backsheet degradation and module output or safety has been identified. However, such a relationship may be expected to become more pronounced with time, affecting system lifetime and ultimately the levelized cost of electricity (LCOE). The observed phenomena have implications for both backsheet product development and array design, especially for modules that utilize newer classes of non-fluoropolymer-based backsheets which are typically more susceptible to environmental degradation.

1. Introduction

Backsheets serve a crucial role in the safe operation of photovoltaic (PV) modules, acting as both a weathering barrier and electrical insulation for the backside of solar cells (Gambogi et al., 2013; Köntges et al., 2014; Oreski and Wallner, 2005; Voronko et al., 2015). Backsheets are typically polymer laminates consisting of a weather-resistant outer layer, an electrically insulating core layer, and an inner layer which promotes adhesion to the solar cell encapsulation. During outdoor exposure, polymeric materials tend to degrade and lose their functionality, which makes the selection of a backsheet for PV modules an important design consideration, especially with the ≥25 year warranties from many manufacturers∗(Jordan and Kurtz, 2013). Therefore, considerable effort must go into understanding backsheet degradation mechanisms, how degradation influences module performance and safety, and ultimately how to predict the service life of polymeric backsheets (Bruckman et al., 2013; Lin et al., 2016; Oreski and Wallner, 2005; Osterwald and McMahon, 2009; Voronko et al., 2015). These are all significant elements for determining warranty periods and the levelized cost of electricity (LCOE) of a system.

The backsheet market is currently dominated by fluoropolymer-based outer layer materials, such as polyvinyl fluoride (PVF) and polyvinylidene fluoride (PVDF), which tend to withstand weathering and fulfill their functional purpose even after 20 years (Bradley et al., 2015; Gambogi et al., 2013; Oreski and Wallner, 2005). However, continued pressure on manufacturers to reduce module cost has led to the development of lower cost non-fluoropolymer-based backsheets, such as those based on polyester or polyamide outer layer materials. The drawback of non-fluoropolymer-based materials is that they must be modified (e.g., by additives) to withstand weathering, and even with

☆ Certain commercial equipment, instruments, or materials are identified in this work in order to adequately detail the experimental procedure. Such identification is not intended to imply recommendation or endorsement by the National Institute of Standards and Technology, nor is it intended to imply that the materials and equipment identified are necessarily the best available for this purpose.

* Corresponding authors.
E-mail addresses: andrew.fairbrother@nist.gov (A. Fairbrother), xiaohong.gu@nist.gov (X. Gu).

https://doi.org/10.1016/j.solener.2018.01.072
Received 11 September 2017; Received in revised form 21 December 2017; Accepted 20 January 2018
0038-092X/ Published by Elsevier Ltd.

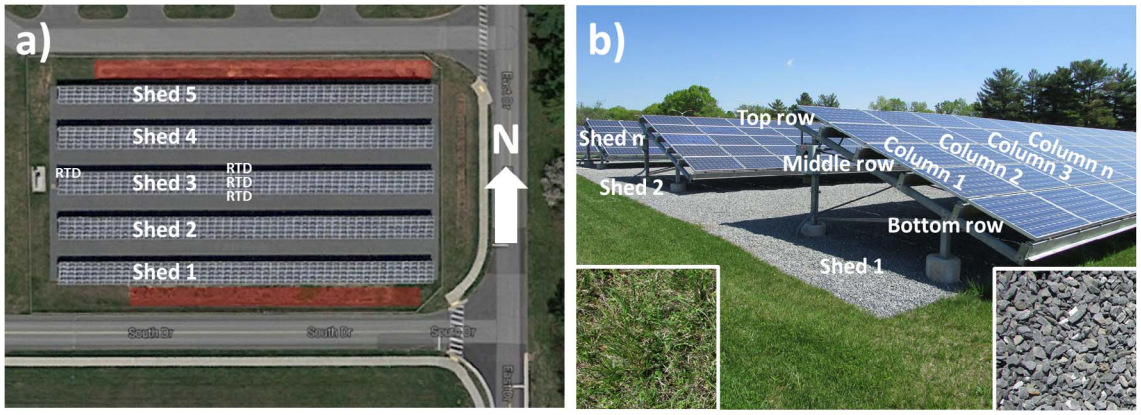

Fig. 1. Layout of the NIST ground-mounted PV array (Google Maps, 2016) (a), and orientation of the modules within the array, including nomenclature labels utilized in this work (shed-row-column) (b). "RTD" in (a) marks the approximate location of modules where backside temperature was recorded, and red boxes show the locations of the bio-retention areas (refer to the online color version). Insets for (b) show the ground cover at the array, including grass and coarse rock.

modification, they may still be more susceptible than fluoropolymers (Bradley et al., 2015; Gambogi et al., 2013; Lin et al., 2016; Oreski and Wallner, 2005). Additionally, because of their more recent commercialization, there are relatively few field studies and a lack of widely accepted testing criteria to help predict their service life. Of the newer outer layer backsheet materials, those based on polyesters such as polyethylene terephthalate (PET) are among the most prominent. Polyethylene naphthalate (PEN), polypropylene, polyimide, and polyamide-based materials are also being considered as potential candidates. Collectively, non-fluoropolymer backsheets constituted nearly 60% of the global backsheet PV market by area in 2014 (Global Market Insights, 2017).

During outdoor exposure there are three main environmental stressors that affect polymer degradation: temperature, humidity, and light (especially ultraviolet (UV)) (Bruckman et al., 2013; Day and Wiles, 1972; Lin et al., 2016; McMahon et al., 1959; Oreski and Wallner, 2005). Additionally, transitory and cyclic variations of these stressors (diurnal, seasonal) can play a role by the addition of thermal-mechanical stresses. Previous field studies tend to focus either on module performance or frontside degradation, and document effects such as power loss, soiling, cell damage, metal contact corrosion, encapsulant discoloration, and frame corrosion (Dechthummarong et al., 2010; Djordjevic et al., 2014; Felder et al., 2014; Gambogi et al., 2015; Hasselbrink et al., 2013; Lopez-Garcia et al., 2016; Quintana et al., 2002; Sánchez-Friera et al., 2011; Skoczek et al., 2009). Comparatively little focus is placed on the backsheets, perhaps because backsheet failure tends occur very late, near the end of the module lifetime, at least for modules with fluoropolymer-based backsheets (i.e. nearly all > 20 year old field-exposed modules).(Köntges et al., 2014) However, this newer class of non-fluoropolymer-based backsheet materials may perform differently over the life of a PV module, and greater scrutiny on backsheet degradation and its effect on module performance and safety is needed. From surveys reporting on backsheet properties, the main degradation and failure indicators include discoloration, delamination, cracks, and burn-marks (from solar cell hot spots).(Dechthummarong et al., 2010; Dunlop and Halton, 2006; Felder et al., 2014; Gambogi et al., 2015; Kato, 2011; Sánchez-Friera et al., 2011) These have the potential to accelerate module degradation, e.g., by allowing liquid moisture ingress which can accelerate corrosion of solar cell metallization (Jaeger et al., 2013; Kempe, 2006; Peike et al., 2012). These failure modes can also pose safety hazards, e.g., by exposing high-voltage discharge points (Dechthummarong et al., 2010; Gambogi et al., 2015; Köntges et al., 2014; Quintana et al., 2002). Ultimately, either of these factors – reduced output and increased safety risks – affect the service life of a module. Therefore, mitigating backsheet degradation is one necessary component of improving PV module reliability and extending module lifetime beyond 25 years to make the LCOE more competitive with conventional power sources such as coal, gas, or nuclear plants, which have > 40 year lifetimes (Tidball et al., 2010).

This work presents results and analysis from a field study of PV module backsheet degradation at a ground-mounted array at the National Institute of Standards and Technology (NIST) in Gaithersburg, Maryland (USA). It is a small utility-scale array installed in August 2012 that consists of 1152 modules having a rated power of 271 kW. The modules are based on front-contact, monocrystalline silicon solar cells, and utilize a PEN-based backsheet. Within the array, significant differences were observed in backsheet degradation characteristics, including color, gloss, and chemical analysis. These differences were shown to be due to gradient exposure conditions that exist within the array, arising from array structural and environmental factors including module location, elevation, and ground cover. In particular, backside UV exposure was found to vary the most and was suspected to cause the observed differences between the backsheets.

2. Materials and methods

2.1. Site and array overview

The ground-mounted PV array is located at the main NIST campus in Gaithersburg, Maryland (USA), with coordinates 39° 07′ 54.7″ N; 77° 12′ 50.8″ W, and an elevation of 136 m. The area has a hot, humid continental climate (Dfa in the Köppen-Geiger classification), which is characterized by a hot summer, and no dry season (Peel et al., 2007). There are 1152 modules (Sharp NU-U235F2) at the site, installed in August 2012, with a total rated DC power of 271 kW (Boyd, 2017). The array is situated on coarse, gray rock (#57 stone, likely granite), and bordered by grass and bio-retention (storm water collection) areas, as seen in Fig. 1. It is divided into five sheds, each with five rows of modules in 48 columns, as shown in Fig. 1b (except shed 5, which contains four rows of modules). The modules are oriented due south at 20° to the ground, and the center-height of the top, middle (third row from bottom), and bottom row modules is approximately 2.2 m, 1.5 m, and 0.9 m, respectively (for shed 5-top row it is 1.9 m). This figure also shows the nomenclature utilized throughout this work (shed-row-column).

2.2. Backsheet properties

Backsheet degradation was monitored using non-destructive techniques, including visual inspection, colorimetry, glossimetry, and Fourier-transform infrared spectroscopy (FTIR). These inspections were made on 24 October and 18 November 2016, corresponding to just over four years of outdoor exposure. Weather on those days was mostly

cloudy and mostly sunny, respectively, with temperatures in the range of 14–18 °C during the time of inspection (late morning/noon). First, visual inspection was made of all the modules to identify evidence of backsheet defects and degradation, and photographs were taken to document their current state. The inspection protocol was based on work by the IEA PVPS Task 13 group, which is used to qualify or quantify visual appearance and damage (Köntges et al., 2014). Second, color (yellow index) and gloss were measured on the backsheet of a subset of 240 modules situated throughout the array with handheld instruments per ISO 7724 and ISO 2813 standards, respectively. Color and gloss measurements were made at three positions within each module: near the junction box, middle of the module, and opposite the junction box. This was to determine the homogeneity of backsheet degradation within a module. Gloss was measured on two separate instruments, though only gloss (60°) from one instrument is reported in the main text. Finally, FTIR spectra were recorded from the backsheet of a subset of 40 modules with a handheld FTIR using an attenuated total reflectance (ATR) attachment. FTIR was measured at two points on each backsheet: near the junction box and in the middle of the module. The initial backsheet properties of these modules is not known because the module is no longer in production. However, a module of the same model with a short field exposure (3 months) has been characterized to provide some indications of how the backsheet has changed over time.

2.3. Backside exposure conditions

Backside exposure conditions, including temperature and irradiance, were measured at different positions in the array, including center and edge modules from the top, middle, and bottom rows. Temperature was recorded since August 2014 with resistance temperature detectors (RTDs) affixed to the backsheet, with a one-minute average of ten-second sampling intervals. The location of these sensors is indicated in Fig. 1a. Irradiance was measured with a crystalline silicon reference cell on the backside center of each module (i.e. 180° from the plane-of-array (POA)). Irradiance measurements were made at noon on 28 April 2017, and weather at the time was sunny with a temperature of about 22 °C. Ground albedo (or reflectivity, the ratio of reflected over incident light) was measured on 5 April 2017 with a pyranometer (range 300 nm to 3000 nm) and UV radiometer (range 295–385 nm) at a height of 0.5 m above grass and rock, the two main types of ground cover at the array. Weather at the time (noon) was sunny, with a temperature around 19 °C. Relative humidity (RH) was not measured at the array, but is not expected to vary significantly throughout the array. A nearby humidity sensor at the NIST weather station recorded a mean and standard deviation of 51% RH ± 21% RH in April 2016 and 66% RH ± 17% RH in September 2016, the driest and wettest months, respectively.

3. Results and discussion

3.1. Visual inspection

Visual inspection of PV backsheets typically yields information about more advanced degradation or defects when compared with optical or spectroscopic measurements, such as cracks, burn-marks, and delamination. Visual inspection of the NIST ground-mounted array shows minor to major discoloration of the backsheets, and no chalking. The texture of most backsheets is like new, while some are a wavy, but not delaminated, along busbars and interconnects (busbar bumps, described next). There is small, localized damage on less than 10% of the backsheets, and two main types of defects or damage were identified: burn-marks and busbar bumps, as seen in Fig. 2. Approximately 3% of the modules in the array have burn marks, and there were typically 1 to 2 affected areas in each of these modules, occupying less than 5% of the backsheet area. Burn-marks are not the result of a backsheet defect, as they are formed by hot spots in the solar cells. In such cases the cell has a higher local temperature, sometimes exceeding hundreds of degrees Celsius, which can damage the backsheet (Kaplani, 2012; Kato, 2011). There were two main types of burn-marks observed in the array, including those in which the backsheet has ruptured ("burn-throughs", presumably higher temperature hot spots) and those in which the backsheet has not ruptured (presumably lower temperature hot spots). Close inspection of the burn-marks in the array reveal physical damage such as scrapes, scratches, and tears in close proximity to many of these marks, as shown by the arrow in Fig. 2a. This physical damage affects less than 5% of the backsheet area, and appears randomly distributed on the affected backsheets. Thus, it is speculated that improper handling prior to and during installation may have damaged some cells, which created hot spots within the modules. This is in contrast to other field surveys, because there is typically no apparent installation damage near the burn-marks (Dechthummarong et al., 2010; Kato, 2011; Sánchez-Friera et al., 2011). Very few burn-marks were found on the bottom row modules compared with the higher modules, possibly because it was easier to handle these modules during installation, resulting in fewer broken cells. Over time these defects will be monitored, as it is possible that the low temperature burn-marks develop into burn-throughs.

The other major backsheet defect observed was busbar and interconnect bumps or ripples. About 5–10% of the modules were affected, and an affected module typically had multiple bumps, which occupy less than 5% of the backsheet area. The origin of these bumps may be due to local delamination or excess ribbon wiring. The bumps were hard to the touch, and if they were due to local delamination or gas buildup one would expect them to be soft or spongy (Kaplani, 2012; Wohlgemuth et al., 2016). The other possibility is excess ribbon wiring for the busbars, which has buckled outward. It is common to have additional ribbon wiring in a module to allow for expansion and contraction within the module, and this defect could be a result of this wiring buckling outward. Busbar bumps were most common on the bottom row modules, and were much rarer on the higher rows, the reasons for which are unclear. Aside from the burn-marks, none of the visually observed defects are expected to create immediate hazards or other concerns. Additional photographs from the visual inspection can be found in Fig. S1 in the Supplementary Material.

While the focus of this work has been on backsheet degradation, it is also worth noting the condition of the other parts of the modules in the array. The junction boxes and module interconnections appeared to be in good condition at the time of the inspection. There was also no visually detectable discoloration of the solar cell encapsulant. There was soiling of the aluminum frame and lower part of the glass, which is typical for field modules. The anti-reflective coating appeared to be inhomogeneous in a small number of modules, giving rise to an "oil-slick" pattern which is particularly visible on overcast days. These oil-slick patterns became noticeable shortly after the array was installed, and are thought to be due to inhomogeneity of the coating process during manufacture. The influence of soiling and anti-reflective coating inhomogeneity on module performance are not studied here, though both may be expected to have some effect on module current (Lopez-Garcia et al., 2016).

3.2. Color and gloss

Polymers tend to yellow and undergo surface erosion over time, thus color (e.g., yellow index) and gloss can be used as proxies for surface degradation and provide more nuanced insights than visual inspection alone. The initial state of these backsheets is not known because the module is no longer in production, however, a module with less UV exposure (3-month field deployment) was available for characterization. This module had low-UV exposure areas where the average and standard deviation for yellow index was −1.1 ± 0.1, and for gloss (60°) was 122 Gloss Units (GU) ± 7 GU, and is considered the

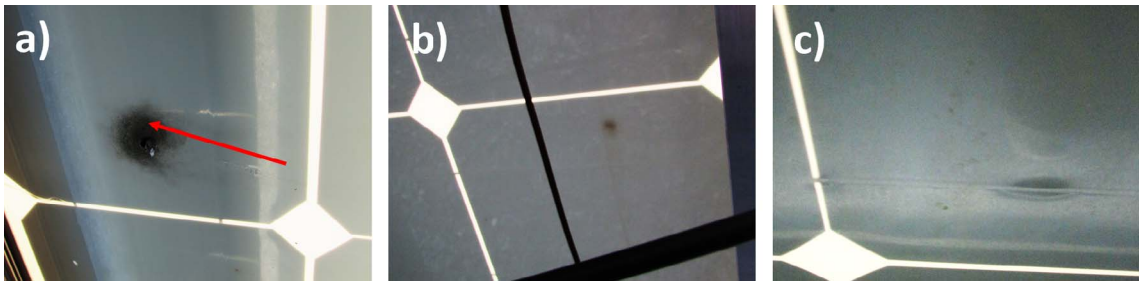

Fig. 2. The two main types of backsheet damage or defects visually observed, including high (a) and low (b) temperature burn-marks, and busbar bumps (c). The arrow in (a) indicates the direction of a scrape.

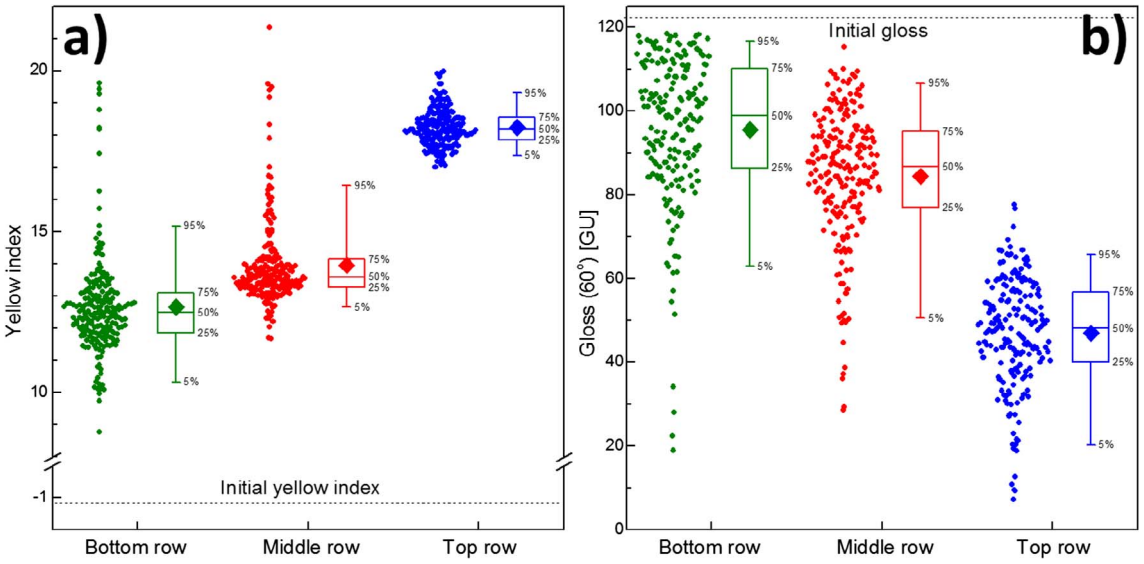

Fig. 3. Yellow index (a) and gloss (60°) (b) for bottom, middle, and top row modules, including mean, median, and various percentile ranges (5%, 25%, 75%, and 95%). Each point represents a single measurement, and there are three measurements per module.

closest available approximation to an initial state for yellowness and gloss. Within the array all backsheets had higher yellowing and lower gloss than the low-UV exposure module, but there was a very wide range of yellow index (9–21) and gloss (6–118 GU) of the backsheets (Fig. S2). Division by module row showed a much clearer pattern of backsheet properties, as seen in Fig. 3. It is unlikely that variation in module manufacturing had given rise to these differences, therefore the exposure conditions must have been different across backside of the modules over the course of > 4 years of operation.

From Fig. 3 it can be seen that backsheets from higher modules (top row) exhibit higher yellow index and lower gloss values. There was a positive skew for yellow index, and negative skew for gloss, which was due to an array edge effect, whereby there is greater weathering of modules at the edge of the array (i.e. in columns 1–3 and 46–48). Average yellowing and gloss values from modules in the center of the sheds and the most extreme edge values are shown in Table 1. The top row modules had a substantially higher average yellow index, 18.1 compared with 12.6 for bottom row modules. Gloss (60°) was also very different, with an average of 50 GU for the top row compared with 91 GU for the bottom row. The middle row modules had somewhat higher yellowing and lower gloss than the bottom row modules, though the difference was much lower when compared with the top row modules. Increased weathering of the edge of array modules – a so-called edge effect – was observed in all sheds, which was most pronounced in the middle and bottom rows.

Table 1
Yellow index and gloss values averaged over the center columns (columns 5–45) (mean ± standard deviation), along with the most extreme edge module values.

Module row	Yellow index		Gloss (60°) [GU]	
	Center	Edge	Center	Edge
Top row (shed 1 to 4)	18.1 ± 0.5	20.4	50 ± 12	12
Top row (shed 5)	13.7 ± 0.5	14.7	103 ± 9	90
Middle row (shed 1 to 5)	13.6 ± 0.7	19.6	87 ± 13	28
Bottom row (shed 1 to 4)	12.6 ± 0.9	19.4	91 ± 12	53
Bottom row (shed 1)	11.8 ± 1.3	19.6	111 ± 6	80

In addition to the module elevation and array edge proximity, the properties for some modules showed a dependence on shed position. This was the case for the shed 5-top row and shed 1-bottom row modules. In the case of the shed 5-top row modules compared with the other top row modules, the yellow index was much lower (13.7 vs. 18.1) and gloss was much higher (103 GU vs. 50 GU), indicating less degradation. It should be highlighted that in shed 5 there are only four modules per column, so the shed 5-top row elevation is about 1.9 m above the ground, compared with 2.2 m for the top row of all other sheds. However, height alone cannot account for the differences, because the degradation appeared less advanced than for the middle row modules which have an even lower mounting height. Therefore, it is thought that differences in ground spectral albedo may also be partly responsible, because shed 5 is partly bordered by grass, which has lower a UV albedo than the rock that borders the other sheds (Blumthaler and Ambach, 1988; Correa and Ceballos, 2008; Feister and Grewe, 1995) Similarly, for the shed 1-bottom row modules, the yellow index was slightly lower than in other sheds (11.8 vs. 12.6), and gloss was higher (111 GU vs. 91 GU). As with shed 5, the shed 1-bottom row modules are partly situated above grass, instead of rock. The shed and edge module

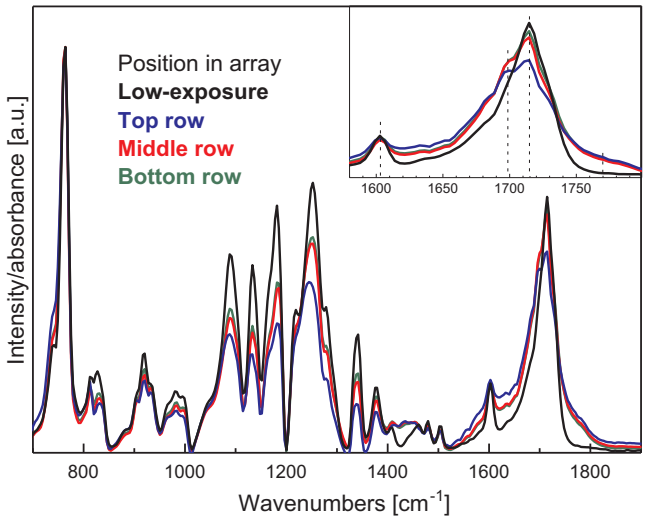

Fig. 4. FTIR spectra from top, middle, and bottom row modules from the center of the sheds. Also shown is a spectrum of a low-exposure PEN backsheet. Inset shows the carbonyl region ($\approx$1700 cm^{-1}). Refer to the online color version for the legend.

effects are more clearly illustrated in Fig. S3 for top, middle, and bottom row modules. Two other factors are discussed in the Supplementary Material, including the presence of outlier modules within the center of the array (Fig. S4), and intramodule homogeneity (Fig. S5).

3.3. Fourier-transform infrared spectroscopy

While color and gloss can quickly provide quantitative values for backsheet surface properties, they cannot be used to determine the composition of the backsheet material and degradation products. FTIR can be used for this, and representative spectra from backsheets in different positions and a low-exposure backsheet are shown in Fig. 4, normalized to the highest band intensity (764 cm^{-1}). The backsheets showed characteristic bands of PEN, such as 764 cm^{-1} (aromatic C—H out-of-plane bend), 1133 cm^{-1} and 1182 cm^{-1} (naphthalene ring vibration), 1252 cm^{-1} (=C—O stretch), and 1715 cm^{-1} (C=O stretch) (Ouchi et al., 1977; Vasanthan and Salem, 1999). Based on the presence of a distinct band at 813 cm^{-1} and band around 831 cm^{-1}, it appears to be semicrystalline α-phase PEN (Vasanthan and Salem, 1999). There were several notable band changes depending on the module position, for instance there was generally a reduction in the main band intensities. The clearest changes occurred in the region around 1700 cm^{-1}, which is related to carbonyl bonds (C=O).(Scheirs and Gardette, 1997) The ratio intensity between 1700 cm^{-1} (carboxylic acid) and 1715 cm^{-1} (ester) increased for the backsheets which had undergone more extensive weathering (i.e. modules in the top row or edge columns). There is also an increase in the high and low wavenumber shoulders of the carbonyls bands, consistent with phenomena observed in controlled photodegradation studies (Scheirs and Gardette, 1997). At the higher wavenumber shoulder, centered around 1770 cm^{-1}, the increase is likely due to the formation of anhydrides. Spectra for the modules at the edges of the array are not shown in Fig. 4, though their spectra indicate more advanced degradation than modules in the same row at the center of the sheds (i.e., higher ratios of 1700 cm^{-1}/1715 cm^{-1} for the same row).

3.4. Backside exposure conditions

Three primary factors are typically studied in the weathering of polymers, including temperature, humidity, and irradiance (especially UV).(Bruckman et al., 2013; Day and Wiles, 1972; Lin et al., 2016; McMahon et al., 1959; Oreski and Wallner, 2005) Humidity levels near the backsheets were not measured, though they are not expected to vary significantly at the length scale of the array. A nearby humidity sensor at the NIST Gaithersburg site recorded a monthly average and standard deviation of 51% RH ± 21% RH for April 2016, and 66% RH ± 17% RH for September 2016, the dried and wettest months for the year, respectively. Backside module temperature was measured at four locations in the array (Fig. 1a), and no significant differences in temperature were measured between the top, middle, and bottom row modules in the center of the array, and the mean daily maximum temperature for May 2016 to August 2016 was about 49 °C. The top row edge module has a slightly cooler temperature of 1–2 °C, most likely due to greater convective cooler. Others have reported small to large temperature differentials within an array, and it may depend on a variety factors, including frame and mounting structure, mounting height, and wind cooling (Farr and Stein, 2014; Kratochvil et al., 2004). Regardless, the findings in this particular array indicate that the difference in backsheet properties reported above were not likely to have arisen from differential temperature profiles of the modules in different rows. More detail on temperature measurements in the array can be found in the Supplementary Material.

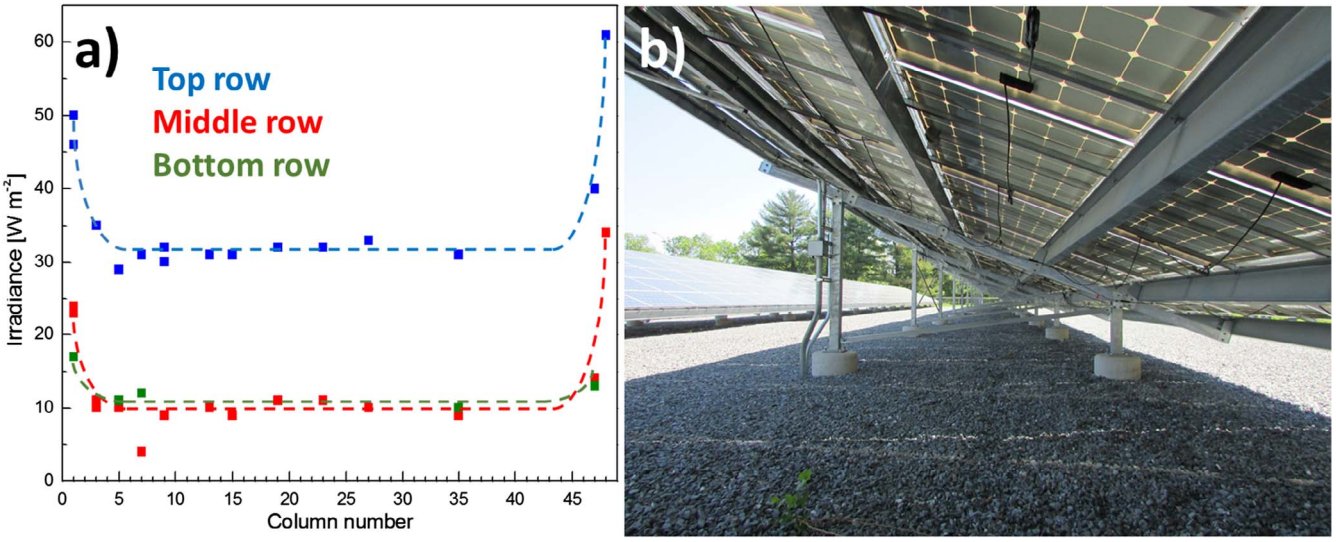

Fig. 5. Backside irradiance around noon on 28 April 2017 at various positions in the array (a). Dashed lines show the trend for each row. A photograph beneath on shed of modules to aid visualization of the backside lighting conditions (b), taken facing east from shed 3-middle row-column 5. Refer to the online color version for the legend.

Table 2
Global plane-of-array (POA) and average backside irradiances (mean ± standard deviation) for top, middle, and bottom row modules from the center and edge of the array around noon on April 28, 2017. These data are not meant to be representative of typical backside exposure conditions and are subject to limitations explained in the main text.

Module row	Irradiance [W m^{-2}]	
	Center	Edge
Global POA	–	965
Top row (shed 1 & 3)	31 ± 1	61
Middle row (shed 1 & 3)	9 ± 2	34
Bottom row (shed 3)	10 ± 1	17

While backside temperature was found to be relatively uniform throughout the array, the backsheet irradiance was not. Fig. 5 shows the backside irradiance measured in the middle of different modules at 180° to the plane-of-array (POA), and a photograph to illustrate the lighting conditions underneath the array. The data are summarized in Table 2. However, these data should not be taken as representative of cumulative backside exposure, for reasons explained shortly. The bifacial PV community has made great progress in modelling and measuring the backside visible light irradiance in arrays, because it is needed to estimate the bifacial gain.(Appelbaum, 2016; Chiodetti, 2015; Dupeyrat et al., 2014; Lindsay et al., 2015) However, application of this knowledge to backsheet irradiance of monofacial PV modules to UV light has yet to be elaborated upon. In the NIST array the measured pattern of irradiance appears similar to the edge module effect observed for yellowing and gloss, and the first 3 columns of modules on either side of the array had the highest irradiance (and consequently, highest yellowing and lowest gloss). The top row was also shown to receive more light than the other rows, though differences between the bottom and middle rows were not significant. Note that the data in Fig. 5 and Table 2 should not be taken as representative of typical exposure conditions for the backsheets, because they come from measurement on a single date (28 April 2017), and irradiance depends strongly on the position of the sun which varies both daily and seasonally (Chiodetti, 2015). Additionally, the detector was a silicon photodiode, which is most sensitive to visible light, and not UV light which is most damaging to polymers. The irradiance presented here is to illustrate that gradient lighting conditions do in fact exist on the backside of the array, a phenomenon which has been reported in the study of bifacial PV modules.

Two main reasons were identified for the variation in backside irradiance, including array structural and environmental factors. Array structural factors include the presence of structures obscuring sunlight (e.g., the array itself, the module frame) (Appelbaum, 2016; Bany and Appelbaum, 1987). Environmental factors include the widely known climatic and cyclic variations of UV irradiance, but also variations in total and spectral albedo of the ground cover and surroundings (Blumthaler and Ambach, 1988; Correa and Ceballos, 2008; Feister and Grewe, 1995). The first is dependent on the array design, including array orientation, length, module spacing, elevation, and tilt angle. The second is dependent on the albedo of the array surroundings, with some example summarized in Table 3. The table shows the total and UV albedo of rock and grass cover at the NIST PV array (these surfaces appear in the insets of Fig. 1b) and of various surfaces which may be present at a PV site, as reported in references (Blumthaler and Ambach, 1988; Correa and Ceballos, 2008; Feister and Grewe, 1995). UV albedo can vary from < 2% for grass, up to 15% for sand and 94% for snow. For installation of an array in any given climate, merely the use of a grass vs. sand ground cover can lead to nearly a ten-fold difference in UV exposure of the backsheets. While fluoropolymer backsheets are inherently robust under UV exposure, non-fluoropolymers are less so and require modification. Thus, the array design, including array structural and environmental factors, becomes especially important for

Table 3
Total and UV albedo for various types of ground cover measured at the NIST PV array and as reported in references (Blumthaler and Ambach, 1988; Correa and Ceballos, 2008; Feister and Grewe, 1995). Total albedo includes the range from 300–3000 nm, while for the UV albedo the NIST measurements shows a portion of UVA + UVB (295–385 nm), while the references report UVB (≈280–320 nm). The data are presented together for illustrative purposes, and are not meant to be compared directly.

Surface	Albedo		Reference
	Total [%]	UV [%]	
Rock (NIST array)	10.4	8.4	This work
Grass (NIST array)	18.9	2.3	This work
Field, land	11.5	2.2	(Blumthaler and Ambach, 1988)
Asphalt	10.6	5.5	(Blumthaler and Ambach, 1988)
Primitive rock	14.4	3.7	(Blumthaler and Ambach, 1988)
Stream sand	23.8	9.1	(Blumthaler and Ambach, 1988)
Alpine pasture	22.5	4.9	(Blumthaler and Ambach, 1988)
New dry snow	87.0	94.4	(Blumthaler and Ambach, 1988)
Loam	–	4.4	(Feister and Grewe, 1995)
Grass	–	1.7	(Feister and Grewe, 1995)
Sand	–	15.2	(Feister and Grewe, 1995)
Snow	–	76.2	(Feister and Grewe, 1995)
Green grass	–	1.1	(Correa and Ceballos, 2008)
Yellow grass	–	1.0	(Correa and Ceballos, 2008)

arrays with modules constructed using non-fluoropolymer backsheets. The erection of simple light blocking structures on the edge and top row of an array could potentially minimize the observed edge and module height effects, though it may also affect the convective cooling of the modules. The selection of low-UV albedo materials for the array surroundings would also reduce the amount of UV exposure to the backsheets. It is interesting to note that studying the influence of array design on backside irradiance is also of interest in the field of bifacial PV (Appelbaum, 2016; Chiodetti, 2015; Dupeyrat et al., 2014; Lindsay et al., 2015). However, in the case of a bifacial PV array the intent is to maximize backside irradiance, rather than minimize it.

3.5. Backsheet degradation and module performance

The main interest of studying backsheet degradation is to understand its effect on various metrics of module performance, such as output power, safety, reliability, and lifetime. To date (summer 2017) none of the modules in the array have experienced performance failures, defined as power loss below 90% of rated power over the first ten years after purchase. Upon observing the unique backsheet degradation patterns in the array the authors sought a link to module performance, but currently they have been unable to establish a clear relationship. Identifying such a relationship is not a trivial task because PV modules and systems are composed of multiple components, each of which has its own unique degradation mechanisms, which may in principle synergistically influence another part. Aside from safety issues due to delamination or burn-throughs, there are no literature reports of a clear correlation between backsheet degradation and module performance. However, only fluoropolymer-based backsheets have been field tested for an extended period of time, and if they fail it tends to be near the end-of-life of a module (i.e. > 20 years), though this may not be the case for the newer class of non-fluorpolymer backsheets. Of the non-fluoropolymer backsheets, only PET has been used for > 10 years, though most PET installations are much younger (Gambogi et al., 2013, 2015). A more thorough understanding of how non-fluoropolymer backsheets degrade in a real-use environment is needed to determine if less critical degradation modes such as yellowing or oxidation result in more catastrophic backsheet or module failure in the future, for instance backsheet cracking and delamination, or causing increased corrosion. Once a clearer relationship between backsheet degradation and module performance is established, a cost-benefit analysis of these materials can be performed, and compared with the field-proven

fluoropolymer technologies. The ground-mounted NIST PV array will continue to be monitored over the coming years, including additional surveys of the backsheet. As the array ages, special attention will be given to modules that are exposed to greater amounts of UV radiation, in particular the top row and edge modules.

4. Conclusions

A survey of the NIST ground-mounted PV array has found that the backside exposure conditions, in particular the irradiance, are highly dependent on array structural and environmental factors of the array design. The presence of light-blocking structures (e.g., the array, buildings, trees) and different ground covers influence the amount of UV light that strikes the backsides of the modules. These differential exposure conditions have given rise to a unique pattern of backsheet degradation, one in which modules near the edge of the array and at higher elevations have undergone more extensive yellowing, gloss-loss, and chemical change. This has implications for the design of arrays with modules that use the comparatively new classes of non-fluoropolymer-based backsheets, such as PET, PEN, or polyamide, which tend to be more susceptible to environmental degradation than fluoropolymer backsheets. No link between module performance (output, safety) and backsheet degradation has been identified so far, though if a correlation exists it might be expected to become more pronounced with time when backsheet cracking and delamination occur.

Conflict of interest

The authors declare no competing financial interests.

Acknowledgement

This work was funded in part by the U.S. Department of Energy, SunShot project, under award number DE-EE0007143. The authors would like to thank the Office of Facilities and Property Management (OFPM) at NIST for allowing access to the PV array.

Appendix A. Supplementary material

Supplementary data associated with this article can be found, in the online version, at http://dx.doi.org/10.1016/j.solener.2018.01.072.

References

Appelbaum, J., 2016. View factors to grounds of photovoltaic collectors. J. Sol. Energy Eng. 138, 064501.
Bany, J., Appelbaum, J., 1987. The effect of shading on the design of a field of solar collectors. Sol. Cells 20, 201–228.
Blumthaler, M., Ambach, W., 1988. Solar UVB-albedo of various surfaces. Photochem. Photobiol. 48, 85–88. http://dx.doi.org/10.1111/j.1751-1097.1988.tb02790.x.
Boyd, M.T., 2017. High-speed monitoring of multiple grid-connected photovoltaic array configurations and supplementary weather station. J. Sol. Energy Eng. 139, 034502.
Bradley, A.Z., Kopchick, J., Hamzavy, B., 2015. Quantifying PV module defects in the service environment. In: Photovoltaic Specialist Conference (PVSC), 2015 IEEE 42nd. IEEE, pp. 1–3.
Bruckman, L.S., Wheeler, N.R., Ma, J., Wang, E., Wang, C.K., Chou, I., Sun, Jiayang., French, R.H., 2013. Statistical and domain analytics applied to PV module lifetime and degradation science. IEEE Access 1, 384–403. http://dx.doi.org/10.1109/ACCESS.2013.2267611.
Chiodetti, M., 2015. Bifacial PV plants: performance model development and optimization of their configuration. KTH Royal Institute of Technology.
Correa, M.de P., Ceballos, J.C., 2008. UVB surface albedo measurements using biometers. Rev. Bras. Geofísica 26, 411–416.
Day, M., Wiles, D.M., 1972. Photochemical degradation of poly (ethylene terephthalate). II. Effect of wavelength and environment on the decomposition process. J. Appl. Polym. Sci. 16, 191–202.
Dechthummarong, C., Wiengmoon, B., Chenvidhya, D., Jivacate, C., Kirtikara, K., 2010. Physical deterioration of encapsulation and electrical insulation properties of PV modules after long-term operation in Thailand. Sol. Energy Mater. Sol. Cells 94, 1437–1440. http://dx.doi.org/10.1016/j.solmat.2010.03.038.
Djordjevic, S., Parlevliet, D., Jennings, P., 2014. Detectable faults on recently installed solar modules in Western Australia. Renew. Energy 67, 215–221. http://dx.doi.org/10.1016/j.renene.2013.11.036.
Dunlop, E.D., Halton, D., 2006. The performance of crystalline silicon photovoltaic solar modules after 22 years of continuous outdoor exposure. Prog. Photovolt. Res. Appl. 14, 53–64. http://dx.doi.org/10.1002/pip.627.
Dupeyrat, P., Lucas, C., Lindsay, A., Plotton, A., Radouane, K., 2014. Investigations on albedo dependency of bifacial PV yield. 29th Eur. Photovolt. Sol. Energy Conf. Exhib. 2900–2903. http://dx.doi.org/10.4229/EUPVSEC20142014-5BV.2.30.
Farr, M., Stein, J., 2014. Spatial variations in temperature across a photovoltaic array. In: Photovoltaic Specialist Conference (PVSC), 2014 IEEE 40th. IEEE, pp. 1921–1927.
Feister, U., Grewe, R., 1995. Spectral albedo measurements in the UV and visible region over different types of surfaces. Photochem. Photobiol. 62, 736–744. http://dx.doi.org/10.1111/j.1751-1097.1995.tb08723.x.
Felder, T.C., Gambogi, W.J., Kopchick, J.G., Peacock, R.S., Stika, K.M., Trout, T.J., Bradley, A.Z., Hamzavytehrany, B., Gok, A., French, R.H., Fu, O., Hu, H., 2014. Optical properties of PV backsheets: key indicators of module performance and durability. In: SPIE Proceedings Volume 9179, Reliability of Photovoltaic Cells, Modules, Components, and Systems VII. http://dx.doi.org/10.1117/12.2062063.
Gambogi, W., Heta, Y., Hashimoto, K., Kopchick, J., Felder, T., MacMaster, S., Bradley, A., Hamzavytehraney, B., Felix, V., Aoki, T., Stika, K., Garreau-Illes, L., Trout, T.J., 2013. Weathering and durability of PV backsheets and impact on PV module performance. p. 88250B–88250B–11. http://dx.doi.org/10.1117/12.2024491.
Gambogi, W., Kopchick, J., Felder, T., MacMaster, S., Bradley, A., Hamzavytehrany, B., Wang, C.F., Hu, H., Garreau-Iles, L., Trout, T.J., 2015. Sequential and weathering module testing and comparison to fielded modules. In: NREL Photovoltaic Reliability Workshop.
Global Market Insights, 2017. Solar PV Backsheet Market Size - Industry Share Analysis Report 2024 (No. GMI2184), 1–453.
Hasselbrink, E., Anderson, M., Defreitas, Z., Mikofski, M., Shen, Y.-C., Caldwell, S., Terao, A., Kavulak, D., Campeau, Z., DeGraaff, D., 2013. Validation of the PVLife model using 3 million module-years of live site data. In: Photovoltaic Specialists Conference (PVSC), 2013 IEEE 39th. IEEE, pp. 0007–0012.
Jaeger, C., Graichen, A., Schoeppel, W., Stollwerck, G., 2013. Polyolefin backsheet and new encapsulant suppress cell degradation in the module. 28th Eur. Photovolt. Sol. Energy Conf. Exhib. 3318–3320. http://dx.doi.org/10.4229/28thEUPVSEC2013-4AV.5.44.
Jordan, D.C., Kurtz, S.R., 2013. Photovoltaic degradation rates—an analytical review. Prog. Photovolt. Res. Appl. 21, 12–29.
Kaplani, E., 2012. Detection of degradation effects in field-aged c-Si solar cells through IR thermography and digital image processing. Int. J. Photoenergy 2012, 1–11. http://dx.doi.org/10.1155/2012/396792.
Kato, K., 2011. PVRessQ!: a research activity on reliability of PV systems from an user's viewpoint in Japan. In: Dhere, N.G., Wohlgemuth, J.H., Lynn, K.W. (Eds.), p. 81120K. http://dx.doi.org/10.1117/12.896135.
Kempe, M., 2006. Modeling of rates of moisture ingress into photovoltaic modules. Sol. Energy Mater. Sol. Cells 90, 2720–2738. http://dx.doi.org/10.1016/j.solmat.2006.04.002.
Köntges, M., Kurtz, S., Packard, C., Jahn, U., Berger, K.A., Kato, K., 2014. Performance and reliability of photovoltaic systems: subtask 3.2: review of failures of photovoltaic modules: IEA PVPS task 13: external final report IEA-PVPS. International Energy Agency, Photovoltaic Power Systems Programme, Sankt Ursen.
Kratochvil, J.A., Boyson, W.E., King, D.L., 2004. Photovoltaic array performance model. Sandia National Laboratories.
Lin, C.-C., Krommenhoek, P.J., Watson, S.S., Gu, X., 2016. Depth profiling of degradation of multilayer photovoltaic backsheets after accelerated laboratory weathering: cross-sectional Raman imaging. Sol. Energy Mater. Sol. Cells 144, 289–299. http://dx.doi.org/10.1016/j.solmat.2015.09.021.
Lindsay, A., Chiodetti, M., Dupeyrat, P., Binesti, D., Lutun, E., Radouane, K., 2015. Key Elements in the Design of Bifacial PV Power Plants. In: Proceedings of the 31st European Photovoltaic Solar Energy Conference and Exhibition. Presented at the 31st European Photovoltaic Solar Energy Conference and Exhibition, pp. 1764–1769. http://dx.doi.org/10.4229/EUPVSEC20152015-5CO.14.4.
Lopez-Garcia, J., Pozza, A., Sample, T., 2016. Long-term soiling of silicon PV modules in a moderate subtropical climate. Sol. Energy 130, 174–183. http://dx.doi.org/10.1016/j.solener.2016.02.025.
McMahon, W., Birdsall, H.A., Johnson, G.R., Camilli, C.T., 1959. Degradation studies of polyethylene terephthalate. J. Chem. Eng. Data 4, 57–79.
Oreski, G., Wallner, G.M., 2005. Aging mechanisms of polymeric films for PV encapsulation. Sol. Energy Polym. Mater. Solar Energy Appl. 79, 612–617. http://dx.doi.org/10.1016/j.solener.2005.02.008.
Osterwald, C.R., McMahon, T.J., 2009. History of accelerated and qualification testing of terrestrial photovoltaic modules: a literature review. Prog. Photovolt. Res. Appl. 17, 11–33. http://dx.doi.org/10.1002/pip.861.
Ouchi, I., Hosoi, M., Shimotsuma, S., 1977. Infrared spectra of poly (ethylene 2, 6-naphthalate) and some related polyesters. J. Appl. Polym. Sci. 21, 3445–3456.
Peel, M.C., Finlayson, B.L., Mcmahon, T.A., 2007. Updated world map of the Köppen-Geiger climate classification. Hydrol. Earth Syst. Sci. Discuss. 4, 439–473.
Peike, C., Hülsmann, P., Blüml, M., Schmid, P., Weiß, K.-A., Köhl, M., 2012. Impact of permeation properties and backsheet-encapsulant interactions on the reliability of PV modules. ISRN Renew. Energy 2012, 1–5. http://dx.doi.org/10.5402/2012/459731.
Quintana, M.A., King, D.L., McMahon, T.J., Osterwald, C.R., 2002. Commonly observed degradation in field-aged photovoltaic modules. In: Photovoltaic Specialists Conference, 2002. Conference Record of the Twenty-Ninth IEEE. IEEE, pp. 1436–1439.
Sánchez-Friera, P., Piliougine, M., Peláez, J., Carretero, J., Sidrach de Cardona, M., 2011. Analysis of degradation mechanisms of crystalline silicon PV modules after 12 years of operation in Southern Europe. Prog. Photovolt. Res. Appl. 19, 658–666. http://dx.

doi.org/10.1002/pip.1083.
Scheirs, J., Gardette, J.-L., 1997. Photo-oxidation and photolysis of poly (ethylene naphthalate). Polym. Degrad. Stab. 56, 339–350.
Skoczek, A., Sample, T., Dunlop, E.D., 2009. The results of performance measurements of field-aged crystalline silicon photovoltaic modules. Prog. Photovolt. Res. Appl. 17, 227–240. http://dx.doi.org/10.1002/pip.874.
Tidball, R., Bluestein, J., Rodriguez, N., Knoke, S., 2010. Cost and Performance Assumptions for Modeling Electricity Generation Technologies.
Vasanthan, N., Salem, D.R., 1999. Structural and conformational characterization of poly (ethylene 2,6-naphthalate) by infrared spectroscopy. Macromolecules 32, 6319–6325. http://dx.doi.org/10.1021/ma990136l.
Voronko, Y., Eder, G.C., Knausz, M., Oreski, G., Koch, T., Berger, K.A., 2015. Correlation of the loss in photovoltaic module performance with the ageing behaviour of the backsheets used: Influence of backsheet on photovoltaic module performance. Prog. Photovolt. Res. Appl. 23, 1501–1515. http://dx.doi.org/10.1002/pip.2580.
Wohlgemuth, J.H., Hacke, P., Bosco, N., Miller, D.C., Kempe, M.D., Kurtz, S.R., 2016. Assessing the causes of encapsulant delamination in PV modules. In: Photovoltaic Specialists Conference (PVSC), 2016 IEEE 43rd. IEEE, pp. 0248–0254.